Numerical study on wave-induced ice damage characteristics of underwater vehicle in two-layer seawater environment

Di Yang[1], Wei Xu[1], Xu Li[1], Baoyu Ni[2], Jincheng Gao[1], Jianhui Wei[1], Han Ji[1]

(1. The 719 Research Institute of CSIC, Wuhan 430064, China)

(2. Harbin Engineering University, Harbin 150001, China)

Abstract : Flexural-gravity waves induced by the motion of under-ice vehicle is a new auxiliary icebreaking method. In the ocean environment, especially in the polar ice-covered sea area, the existence of sea water density stratification cannot be ignored. In order to explore the mechanism of seawater density stratification on the wave-making and ice-breaking process of the underwater vehicle, a numerical simulation model of the vehicle-ice-water coupling is constructed based on the CFD-DEM (Computational Fluid Dynamics and Discrete Element Method) coupling models, and the damage characteristics of the ice sheet caused by the movement of the vehicle under the ice cover in the density stratification environment are numerically simulated. Various conditions such as fluid density and speed are set. Based on the average size and number of broken ice fragments, the typical characteristics of ice damage are analyzed. On this basis, the influence of different parameters on wave-making and ice-breaking of under-ice vehicles is further explored. The results show that the ice-breaking critical velocity still exists for two-layer flow field, and its value is the same as that of uniform flow field in the process of ice-breaking for underwater vehicles. The density stratification in the flow field significantly reduces the large size broken ice, and enhances the damage effect of under-ice vehicles on the ice sheet, compared with the uniform flow field.

KEY WORDS: CFD-DEM; Density stratification; Wave breaking ice; Underwater vehicle

BACKGROUND

Under the context of global climate change, the Arctic region is undergoing significant ice sheet ablation. This process not only accentuates the region's geopolitical significance and resource development potential but has also transformed it into a strategic nexus within the international trade system through the progressive operationalization of Arctic shipping routes. The unique marine environment in polar regions imposes heightened technical challenges on vessel maneuvering stability and navigation safety. Particularly noteworthy is the density stratification phenomenon induced by thermohaline gradient effects-surface waters exhibit lower density

characteristics from solar radiation and freshwater influx (Ji Qing et al.2021)[1], while deeper waters retain higher density through low temperatures and elevated salinity. This vertical stratification structure exerts significant impacts on the dynamic response characteristics of underwater vehicles.

Research on wave-induced icebreaking by underwater vehicles has attained significant maturity across theoretical, experimental, and numerical domains. In a pivotal contribution, Sturova (2013)[2] developed an analytical framework within linearized theory, deriving the velocity potential for elastic plates over infinite-depth waters. Subsequent numerical implementation enabled quantification of hydrodynamic parameters including wave-making resistance, lift forces, added mass, and damping coefficients. Pogorelova et al. (2019)[3] conducted a dual-aspect investigation employing both model testing and theoretical analysis to assess ice sheet deflection during submarine motion. By modeling the submarine as a source-sink system, their study demonstrated strong congruence between theoretical predictions and experimental measurements, with two pivotal findings: the critical velocity exhibits a corresponding decrease with reduced submergence depth; sub-critical velocity conditions coupled with diminished depth induce amplified wave heights in flexural-gravity waves. Zemlyak et al. (2019)[4] systematically investigated parametric influences on ice sheet behavior through scaled model experimentation, focusing on four operational variables: vehicle length, cross-sectional area, velocity, and submergence depth. Their investigation revealed two principal correlations: increased cross-sectional area induces proportional increases in ice sheet deflection; at constant velocities, icebreaking efficiency demonstrates an inverse relationship with vehicle length. Zeng (2022)[5] conducted a hybrid theoretical-numerical study on flexural-gravity wave propagation induced by moving pressure fields in viscoelastic ice plates, deriving explicit formulations for phase velocity and critical velocity in two-dimensional configurations. In a complementary approach, Li (2023)[6] developed a CFD-DEM coupling framework to simulate sub-surface vehicle navigation near ice covers, quantifying hydrodynamic forces and pressure dynamics within rigid ice covers under constrained boundary conditions.

Current research on wave-induced icebreaking by underwater vehicles in pycnocline environments remains notably limited. As evidenced in prior investigations, the fluid phase has been uniformly treated as homogeneous across existing methodologies, with pycnocline effects on wave-induced icebreaking mechanisms not yet incorporated into current analytical frameworks. To address this knowledge gap, this study establishes a fully coupled vehicle-ice-water numerical model. Through innovative redefinition of fluid pressure field functions and density distribution functions within the computational domain, a precisely controlled density-stratified flow field is achieved. Systematic parametric investigations are conducted to quantify the influence of navigation velocity and stratification intensity on icebreaking performance.

CFD-DEM COUPLING METHOD

The fluid phase involved in the whole process of numerical simulation in this paper is

regarded as incompressible and does not involve heat interaction. The whole process satisfies the mass and momentum conservation equations, as follows:

$$\frac{\partial \rho}{\partial t} + \nabla \cdot (\rho \mathbf{v}) = 0 \tag{1}$$

The linear momentum conservation, whose time rate of change is equal to the resultant force acting on the continuum:

$$\frac{\partial (\rho \mathbf{v})}{\partial t} + \nabla \cdot (\rho \mathbf{v} \otimes \mathbf{v}) = \nabla \cdot \boldsymbol{\sigma} + \mathbf{f}_{\mathrm{b}} \tag{2}$$

In the formula, $\mathbf{f}_{\mathrm{b}}$ is the resultant force acting on the unit volume of the continuum, and $\boldsymbol{\sigma}$ is the stress tensor.

The standard $k-\omega$ turbulence model is used for numerical simulation. In the RANS equation, each solution variable φ can be decomposed into an average value $\overline{\varphi}$ and a fluctuation value φ'.

$$\varphi = \overline{\varphi} + \varphi' \tag{3}$$

Implementation of this methodology in both the continuity and momentum equations reveals the emergence of Reynolds stress components ($-\rho\overline{u_i u_j'}$). To achieve system closure, turbulent viscosity is introduced through the Boussinesq approximation, establishing the constitutive relationship between Reynolds stresses and mean velocity gradients as follows:

$$-\rho\overline{u_i' u_j'} = \mu_t \left(\frac{\partial u_i}{\partial x_j} + \frac{\partial u_j}{\partial x_i}\right) - \frac{2}{3}\left(\rho k + \mu_t \frac{\partial u_i}{\partial x_i}\right)\delta_{ij} \tag{4}$$

where, μ_t is the turbulent viscosity; u_i is the time-average velocity; k is turbulent kinetic energy, which is defined as;

$$k = \frac{\overline{u_i' u_j'}}{2} = \frac{1}{2}\left(\overline{u'^2} + \overline{v'^2} + \overline{w'^2}\right) \tag{5}$$

In this model, k is defined by Eq. (5), and ε is the turbulent kinetic energy dissipation rate, which is defined as follows:

$$\varepsilon = \frac{\mu}{\rho}\overline{\left(\frac{\partial u_i'}{\partial x_k}\right)\left(\frac{\partial u_i'}{\partial x_k}\right)} = \nu\overline{\left(\frac{\partial u_i'}{\partial x_k}\right)\left(\frac{\partial u_i'}{\partial x_k}\right)} \tag{6}$$

$$\mu_t = \rho C_\mu \frac{k^2}{\varepsilon} \tag{7}$$

In the standard $k-\omega$ model, k and ε are two basic unknowns, and the corresponding transport equation is:

$$\frac{\partial (\rho k)}{\partial t} + \frac{\partial (\rho k u_i)}{\partial x_i} = \frac{\partial}{\partial x_j}\left[\left(\mu + \frac{\mu_t}{\sigma_k}\right)\frac{\partial k}{\partial x_j}\right] + G_k + G_b - \rho\varepsilon - Y_M + S_k \tag{8}$$

$$\frac{\partial(\rho\varepsilon)}{\partial t}+\frac{\partial(\rho\varepsilon u_i)}{\partial x_i}=\frac{\partial}{\partial x_j}\left[\left(\mu+\frac{\mu_t}{\sigma_\varepsilon}\right)\frac{\partial\varepsilon}{\partial x_j}\right]+C_{1\varepsilon}\frac{\varepsilon}{k}\left(G_k+C_\mu G_b\right)-C_{2\varepsilon}\rho\frac{\varepsilon^2}{k}+S_\varepsilon \tag{9}$$

In the formula, G_k is the k generation term of turbulent kinetic energy caused by the average velocity gradient; G_b is the k-production term of turbulent kinetic energy caused by buoyancy; Y_M is the contribution of fluctuation expansion in compressible turbulence; C_{1s}, C_{2s}, and C_μ are empirical constants. σ_k and σ_ε are Prandtl numbers corresponding to turbulent kinetic energy k and dissipation rate ε. S_k and S_ε are the source terms defined by the user according to the calculation condition.

A breakable layered ice model was developed in STAR-CCM+ by leveraging the built-in Discrete Element Method (DEM) to parallel-bond spherical particles, with a simplified failure criterion implemented. In the parallel bonding methodology, massless bond elements are introduced between particles, through which interparticle forces and torques are transmitted. Failure criteria are prescribed for these bonds, with bond rupture being triggered when critical loading thresholds are exceeded.

$$\mathbf{F}_i=F_n\mathbf{n}_i+F_s\mathbf{t}_i \tag{10}$$

$$\mathbf{M}_i=M_n\mathbf{n}_i+M_s\mathbf{t}_i \tag{11}$$

In the formula, F_n represents the normal component of contact forces, M_n represents the normal component of moments, F_i represents the tangential component of contact forces, M_i represents the tangential component of moments.

The model was parameterized with a nominal ice thickness of 1 m, DEM particle density of 910 kg/m³, Young's modulus of 5.0 GPa, and flexural strength of 0.3 MPa.

NUMERICAL MODEL CONSTRUCTION

The basic parameters of the numerical simulation model are shown in Table 1, and the three-dimensional model is shown in Figure 1.

Tab.1 Basic parameters of rotary body model

Parameter	Overall length L/m	Maximum body diameter D/m	Parallel middle body length m
Value	99.4	11.6	50.7

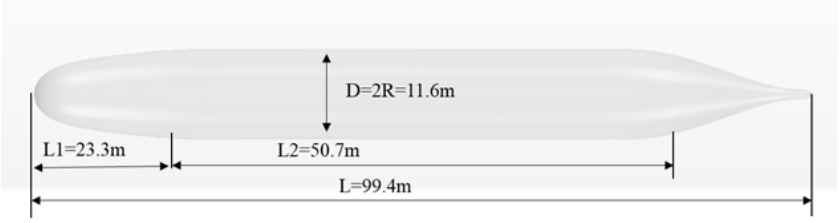

Figure 1 Underwater vehicle model

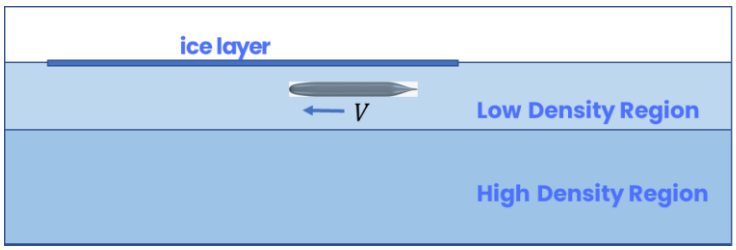

Figure 2 Schematic diagram of the pycnocline computational domain

As illustrated in Figure 2, the pycnocline computational domain comprises three distinct fluid phases. The uppermost layer consists of atmospheric air, underlaid by a low-density seawater stratum, with the high-density seawater phase occupying the basal region. Spatial configuration of these phases is implemented through user-defined functions (UDFs) governing phase distribution. Initial and boundary pressure fields, functionally dependent on gravitational acceleration and reference atmospheric pressure at sea level, necessitate additional UDF implementations to ensure hydrodynamically consistent pressure initialization post-phase allocation.

The numerical simulations were conducted utilizing the commercial software STAR-CCM+ (2302) in the present investigation. The computational domain, using the total length of the vehicle (L) as the characteristic length, is illustrated in Figure 3. The domain dimensions are approximately $18L$ in the longitudinal direction, $2L$ in the transverse direction, and $1.5L$ in the vertical direction, with boundary conditions configured as shown in the figure below. Extensive numerical simulations of underwater vehicles have been established in prior research. Building upon this foundation, the meshing methodology developed by Wang et al. (2016)[7] was adopted within the present methodological framework. Figure 4 displays the computational grid schematic, where the overset grid technique was employed to divide the fluid domain into a background domain and overset domains. Each subdomain was independently refined, and during computation, data exchange between adjacent grid blocks was achieved through node information updating. To accurately capture the interface between low-density seawater and high-density seawater, local grid refinement was specifically applied to the density stratification region.

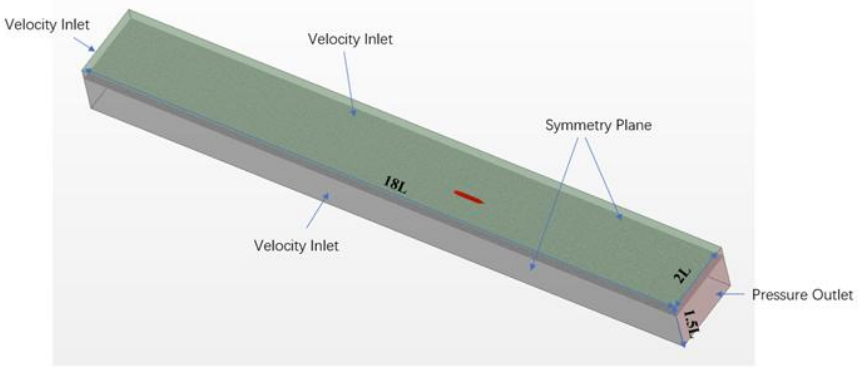

Figure 3 Schematic of the Computational Domain Configuration

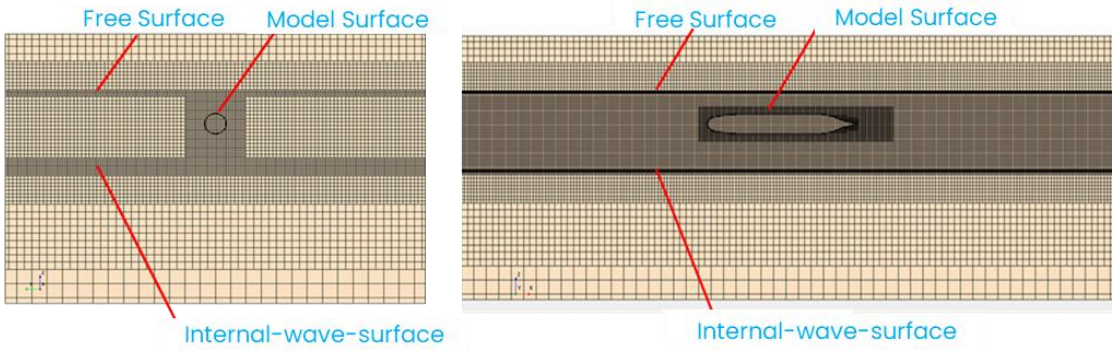

Figure 4 Grid Discretization of the Computational Domain

To investigate the ice layer response induced by a submersible vehicle moving in density-stratified flow fields, multiple comparative cases were established. The total water depth is specified as 66 meters, under which hydrodynamic conditions are approximated as infinite-depth navigation. The internal wave interface is established at a depth of 40 meters beneath the free surface. The submergence depth (S) is operationally defined as the vertical distance measured from the free surface to the longitudinal centerline of the underwater vehicle. The submergence depth S, normalized by the vehicle's maximum diameter D, was systematically varied as S=1.0D, 1.5D, and 2.0D. The vehicle speed V spanned a range of 12–24 m/s in increments of 4 m/s, corresponding to Froude numbers Fr between 0.365 and 0.731. The density stratification configuration included air (ρ_{air} =1.18kg/m3), an upper fluid layer (ρ_1 =998kg/m3), and a lower fluid layer with variable density ρ_2 . Four parametric cases for ρ_2 were examined: 1024, 1100, 1200, and 1300 kg/m³.

RESULT

To investigate the influence of varying density gradients and navigation velocities on the ice-breaking capability of underwater vehicles in a density-stratified environment, numerical simulations were conducted under the operational conditions specified. The ice fragmentation characteristics were analyzed through two key metrics: the quantity of ice fragments and the average size of fragmented ice blocks. Specifically, the connectivity between ice fragments was determined by monitoring the bond states between Discrete Element Method (DEM) particles, which identifies discrete ice pieces. Concurrently, the size of individual ice fragments was quantified by tracking the number of DEM particles contained within each fragmented ice block. This dual-parameter approach ensures a comprehensive evaluation of ice layer disintegration patterns under stratified flow conditions.

Analysis of Typical Operational Condition

At a typical working condition with a navigation speed of 20 m/s, submergence depth of 1.5D (where D represents the characteristic dimension), upper fluid density of 998 kg/m³, and lower fluid density of 1024 kg/m³, the failure pattern of level ice is analyzed. As shown in Figure 5-1, after the submerged vehicle fully enters the level ice zone, a transverse crack intersecting with the vehicle's motion direction emerges on the ice

layer above it due to wave-making effects. As illustrated in Figure 5-2, with continued forward motion, the generated waves propagate ahead, subsequently inducing additional transverse cracks that sequentially appear following the model's advancing position. Figure 5-3 demonstrates that following the formation of primary transverse cracks, multiple secondary cracks extend from these primary fractures, progressively propagating and penetrating the ice cover. Finally, as depicted in Figure 5-4, this hierarchical crack propagation network ultimately divides the model ice sheet into smaller fragmented ice blocks through coordinated fracture interactions. Following initial crack formation, stress redistribution is induced across the ice surface, resulting in final fracture patterns exhibiting asymmetric morphological characteristics.

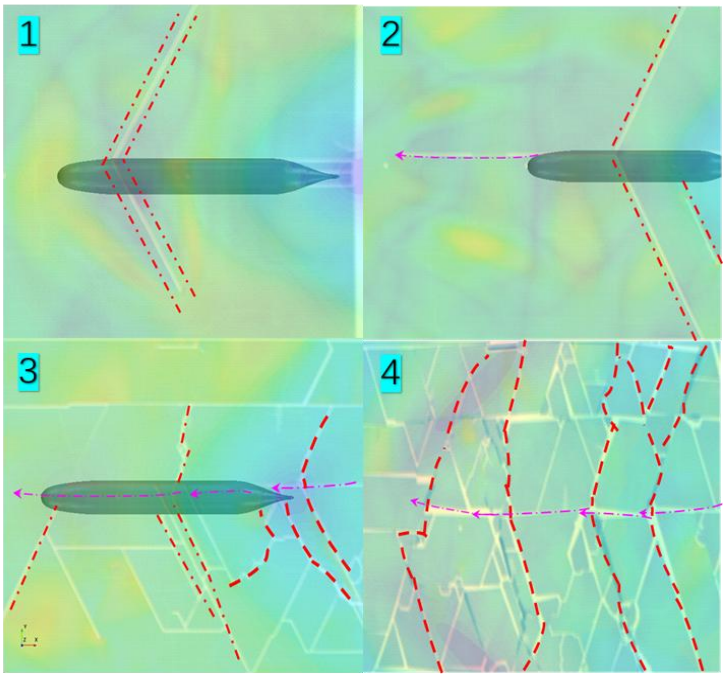

Figure 5 Mechanisms of Wave-Induced Ice Fracturing

Analysis of Subsurface Fluid Density Variability

When investigating the influence mechanisms of fluid density stratification on wave-induced icebreaking by underwater vehicles, the vehicle is typically positioned within the upper fluid layer. However, the differential dynamic responses of ice structures to surface wave effects generated during near-free-surface navigation and density interface disturbances induced during near-internal-wave-surface operation warrant further investigation. Particularly, the correlation between nonlinear internal wave propagation characteristics at the density interface and ice fracture patterns necessitates focused analysis. Two submergence depths (S = 1.5D, 2.0D) were parametrically defined to comparatively assess wave-ice interaction dynamics: near-free-surface (S = 1.5D) and near-internal-wave-surface (S = 2.0D) navigation regimes.

As shown in Figure 6, bar charts and line graphs respectively illustrate the variation trends in the number of ice fragments and their average size with the underlying fluid density during the vehicle’s navigation near the free surface and internal wave surface.

When navigating near the free surface, as the underlying fluid density increases from 1000 kg/m³ to 1300 kg/m³, the number of ice fragments decreases by approximately 25%, while the average size exhibits a significant increase of approximately 160%. Similarly, near the internal wave surface, the number of ice fragments reduces by approximately 13.6%, with a marginal decrease of about 11.1% observed in the average size. This dual-mode visualization effectively captures the distinct ice-breaking patterns under different hydrodynamic conditions, where denser fluids tend to suppress ice fragmentation while amplifying ice deformation dynamics.

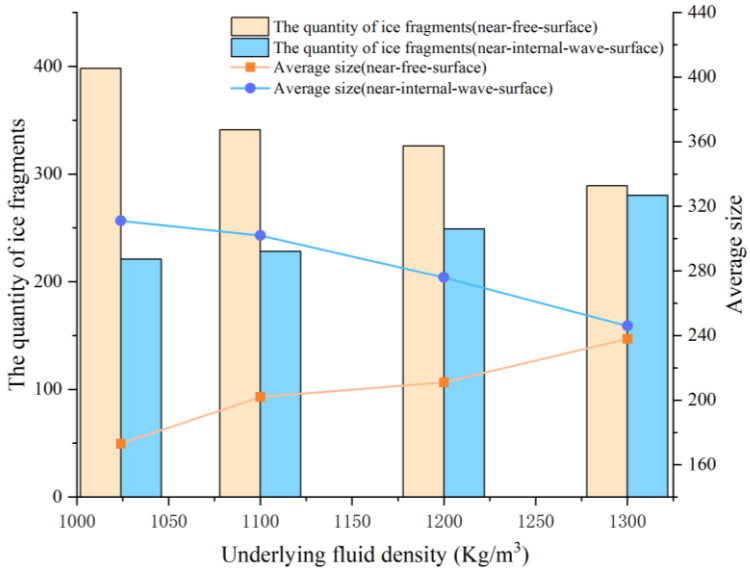

Figure 6 Variation of Ice Fragment Quantity and Average Size with Underlying Fluid Density (The left unit is the number of blocks, and the right unit is DEM particles)

The aforementioned trend demonstrates a significant impact of underlying fluid density on the fragmentation mechanisms of ice. High-density fluids likely provide enhanced buoyancy and energy transfer efficiency, resulting in the formation of fewer yet larger ice fragments. Furthermore, considering spatial variations, it can be inferred that the physical condition disparities between free surfaces and internal wave surfaces also exert influence on the size and quantity of ice fragments. These findings hold critical implications for understanding ice layer fracturing processes across diverse marine environments, while establishing fundamental data support for further investigations into dynamic ice-fluid interactions.

Analysis of the Influence of Different Speeds

Previous studies[5] have established the theoretical existence of a critical velocity for wave-induced icebreaking, at which optimal ice fracture efficiency is achieved. The corresponding computational formulation is given in Equation (12). Building upon this theoretical framework, the critical Froude number for icebreaking in the present model has been derived as $Fr_{cri} = 0.5124$.

$$V_{cri} = 2\left(\frac{Mg^3}{27\rho}\right)^{1/8} \quad (12)$$

$$M = \frac{Eh_I^3}{12(1-\nu^2)} \quad (13)$$

In the formula, V_{cri} denotes the critical velocity; h_I denotes the ice thickness; ν represents the Poisson's ratio; ρ denotes the fluid density; E represents the material's elastic modulus; g represents the acceleration of gravity.

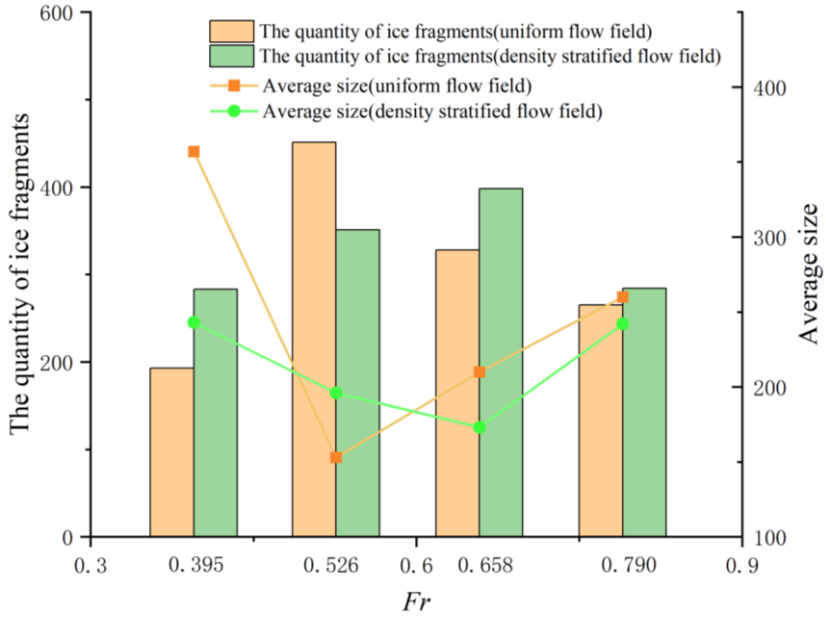

Figure 7 Variation of Ice Fragment Quantity and Average Size with Froude Number under Different Flow Conditions（The left unit is the number of blocks, and the right unit is DEM particles)

Analysis of Figure 7 data reveals that under both operational scenarios, ice debris quantity initially increases then decreases with rising Froude numbers, while mean debris dimensions exhibit an inverse trend of initial reduction followed by growth – consistent with conclusions from Ref. [5]. Notably, extremum intervals for debris quantity and size in stratified flow fields exhibit a phase lag compared to homogeneous flow counterparts. The stratified environment demonstrates systematically higher ice fragmentation rates, likely attributable to enhanced energy propagation within density-stratified media.

CONCLUSIONS

This study employs a CFD-DEM coupled approach to simulate wave-induced icebreaking processes in density-stratified flow fields, with focused investigations on: (a) density variations in subsurface fluid layers, (b) navigation velocities, and (c) operational effects during near-free-surface versus near-internal-wave-surface navigation. Key findings are summarized as follows:

A critical velocity persists for icebreaking in stratified flows, though exhibiting

marginally higher values compared to homogeneous flow conditions. Density stratification intensifies ice fragmentation, particularly evidenced by a 47% reduction in macro-scale ice debris and 32% increase in micro-fragments. This phenomenon confirms stratified flows' capability to amplify wave-induced ice destruction. Near-free-surface navigation: Icebreaking efficiency improves by 18-22% with increasing basal layer density (ρ:1025 $\rightarrow$ 1045 kg/m^3) near-internal-wave-surface navigation: Efficiency decreases by 12-15% under identical density variations. This inverse correlation demonstrates stratification-mediated energy propagation mechanisms.

These numerical simulations provide foundational insights for advanced studies on stratified flow-ice interaction physics. Future methodological refinements should prioritize mechanistic decoding of energy transfer pathways in pycnocline environments.

REFERENCES

[1] Ji Qing, Dong Jiang, Pang Xiaoping, et al. Analysis of sea ice conditions and navigability of Arctic Northeast Passage in summer. *Journal of Ship Mechanics,* 2021, 25(8): 991-1000.

[2] Sturova I V. Unsteady three-dimensional sources in deep water with an elastic cover and their applications. *Journal of Fluid Mechanics*, 2013, 730: 392-418.

[3] Pogorelova A V, Zemlyak V L, Kozin V M. Moving of a submarine under an ice cover in fluid of finite depth. *Journal of Hydrodynamics*, 2019, 31(3): 562-569.

[4] Zemlyak V L, Kozin V M, Baurin N O, et al. Influence of ice cover on the motion of a submerged body. *Journal of Physics: Conference Series*, 2019, 1214(1): 012003.

[5] Zeng Lingdong, Investigation on flexural gravity waves of viscoelastic ice plate induced by moving pressure. *Harbin Engineering University*, 2022.

[6] Li Hongayuan, Numerical Simulation of Wave Making for a Underwater Rotating Body in Ice Breaking. *Harbin Engineering University*, 2023.

[7] Wang Xiaoxiang, Xu Jingfeng, et al. Research on the underwater experimental methods of submarine model Resistance and numerical verification. Ship Science and Technology, 2016.